Science Advances
AAAS

Supplementary Materials for

Single-site Pt-doped RuO_2 hollow nanospheres with interstitial C for high-performance acidic overall water splitting

Juan Wang, Hao Yang, Fan Li, Leigang Li, Jianbo Wu, Shangheng Liu, Tao Cheng, Yong Xu*, Qi Shao, Xiaoqing Huang*

*Corresponding author. Email: yongxu@gdut.edu.cn (Y.X.); hxq006@xmu.edu.cn (X.H.)

Published 2 March 2022, *Sci. Adv.* **8**, eabl9271 (2022)
DOI: 10.1126/sciadv.abl9271

This PDF file includes:

Figs. S1 to S29
Tables S1 to S3
References

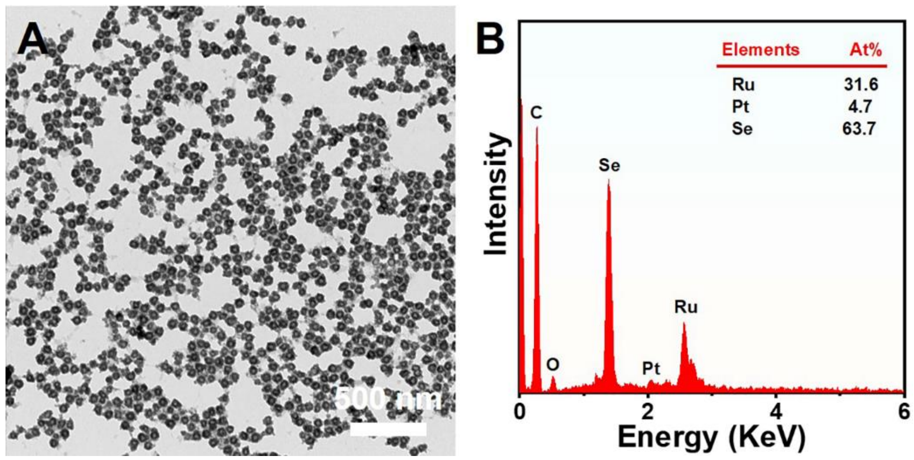

Fig. S1. Morphological and structural characterizations of PtRuSe HNSs. (A) TEM image and (B) SEM-EDS spectrum of PtRuSe HNSs.

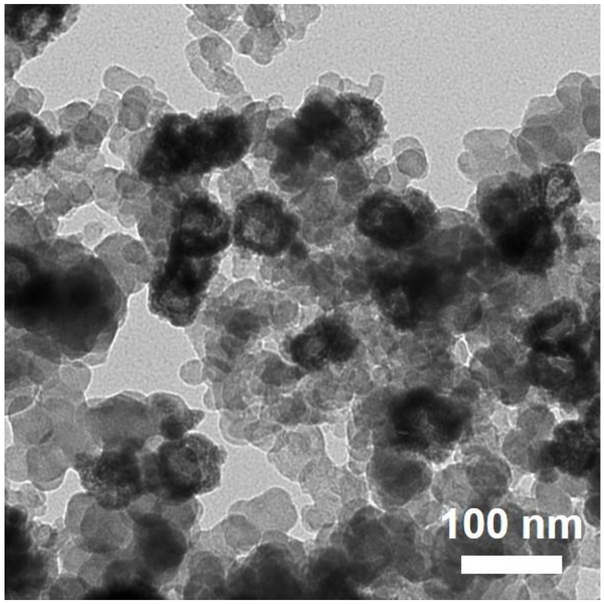

Fig. S2. TEM image of carbon supported PtRuSe HNSs. The dark structures are PtRuSe HNSs in the TEM image.

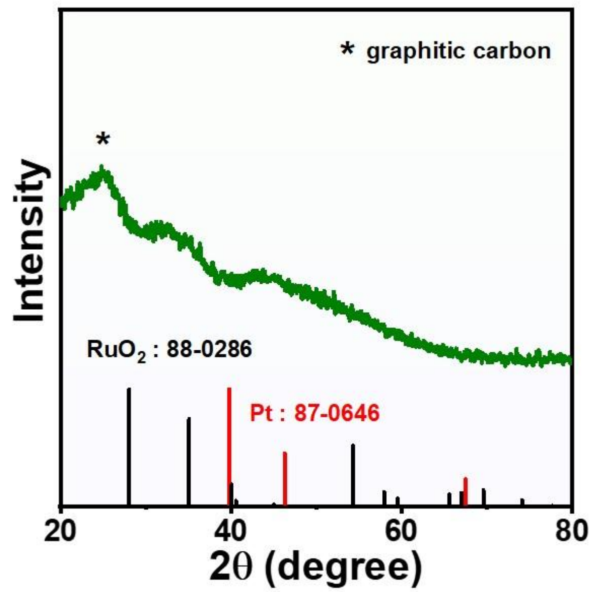

Fig. S3. Structural analysis of SS Pt-RuO_2 HNSs. XRD pattern of carbon supported PtRuSe HNSs. The references of RuO_2 and Pt are inserted in XRD pattern.

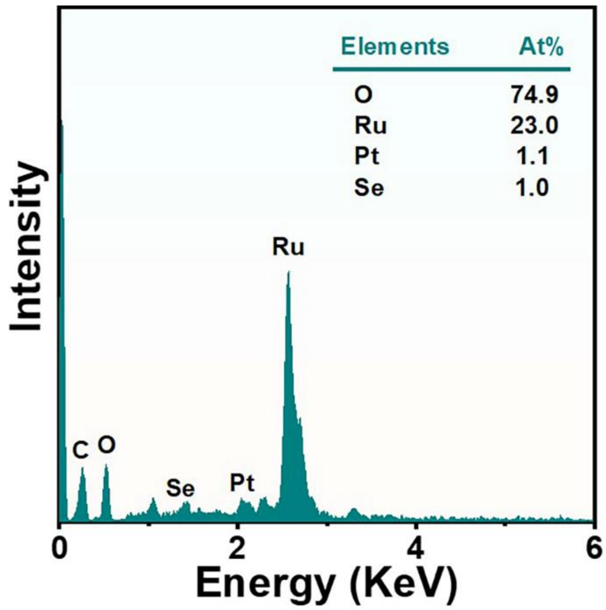

Fig. S4. Structural analysis of SS Pt-RuO_2 HNSs. SEM-EDS spectrum of SS Pt-RuO_2 HNSs.

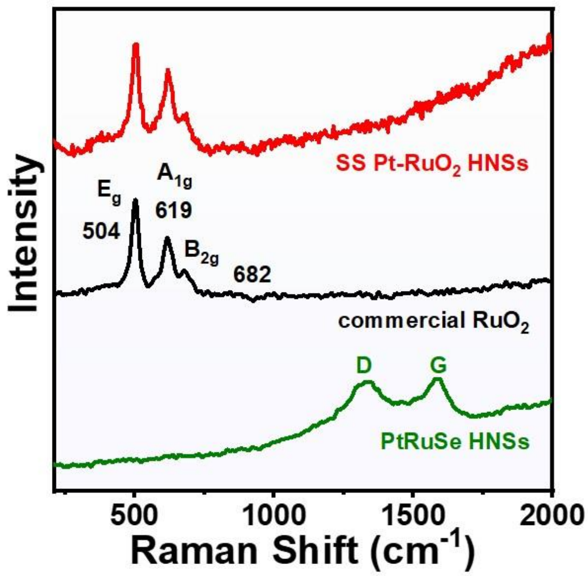

Fig. S5. Structural analysis of SS Pt-RuO_2 HNSs. Raman spectra of SS Pt-RuO_2 HNSs, commercial RuO_2 and carbon supported PtRuSe HNSs.

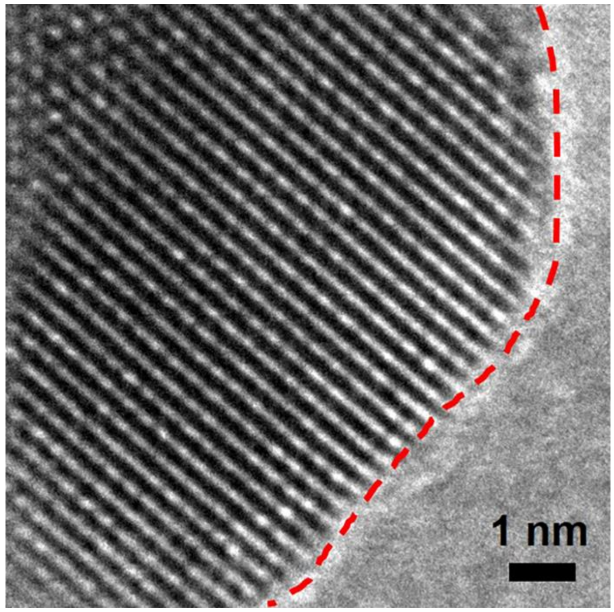

Fig. S6. Structural analysis of SS Pt-RuO_2 HNSs. HRTEM image of SS Pt-RuO_2 HNSs.

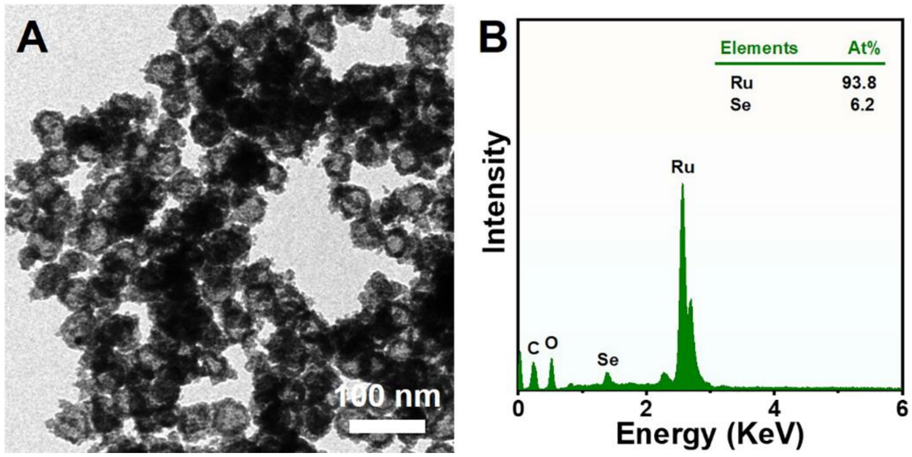

Fig. S7. Morphological and structural analysis of RuO_2 HNSs. (A) TEM image and (B) SEM-EDS spectrum of RuO_2 HNSs.

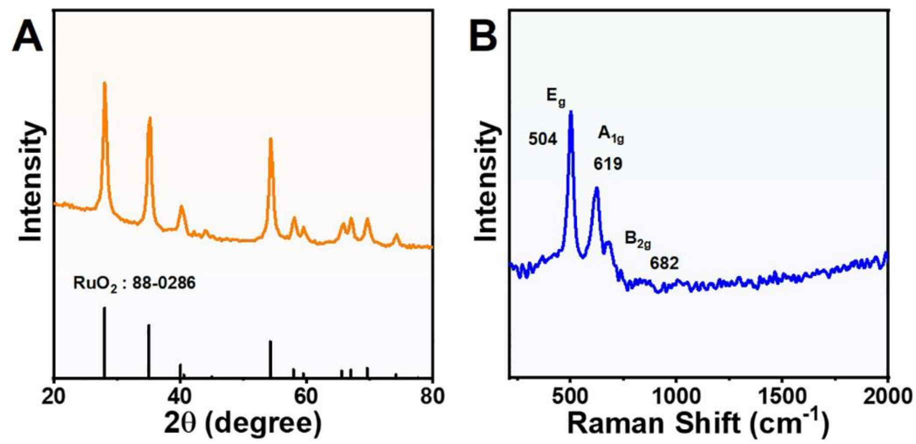

Fig. S8. Morphological and structural analysis of RuO_2 HNSs. (A) XRD pattern and (B) Raman spectrum of RuO_2 HNSs.

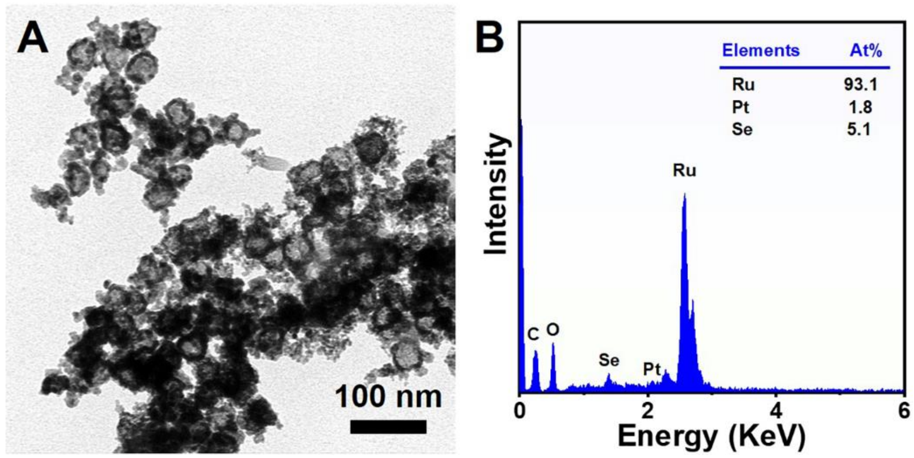

Fig. S9. Morphological and structural analysis of 2% Pt-RuO_2 HNSs. (A) TEM image and (B) SEM-EDS spectrum of 2% Pt-RuO_2 HNSs.

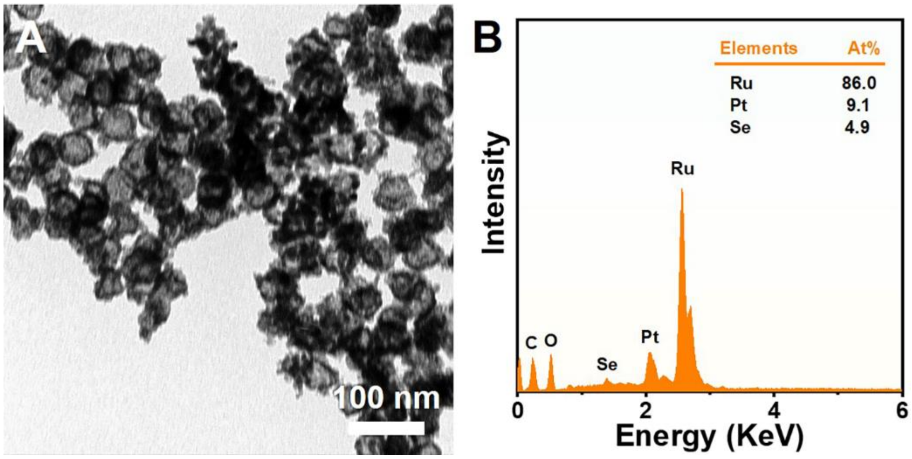

Fig. S10. Morphological and structural analysis of 10% Pt-RuO_2 HNSs. (A) TEM image and (B) SEM-EDS spectrum of 10% Pt-RuO_2 HNSs.

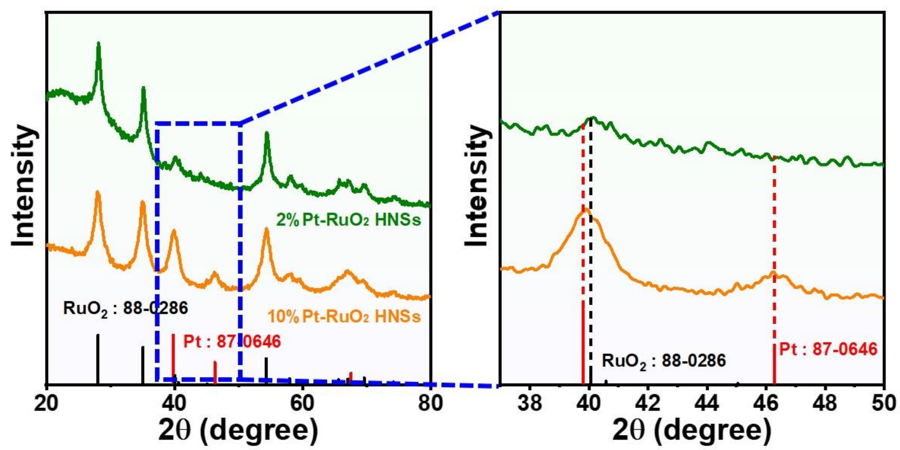

Fig. S11. Structural analysis. XRD patterns of 2% Pt-RuO_2 HNSs and 10% Pt-RuO_2 HNSs.

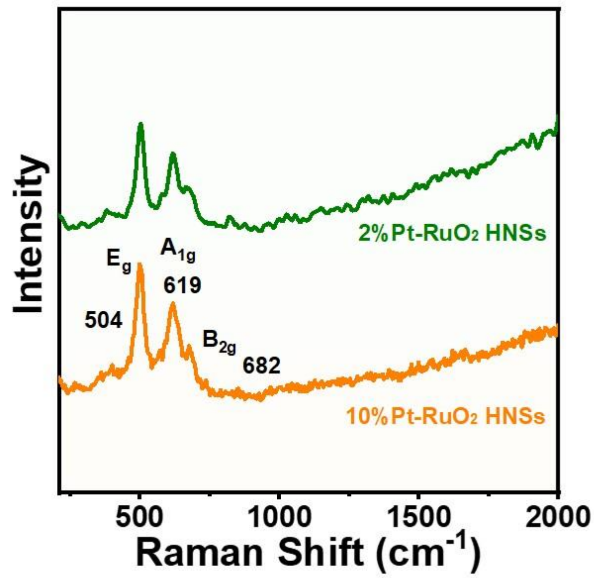

Fig. S12. Structural analysis. Raman spectra of 2% Pt-RuO_2 HNSs and 10% Pt-RuO_2 HNSs.

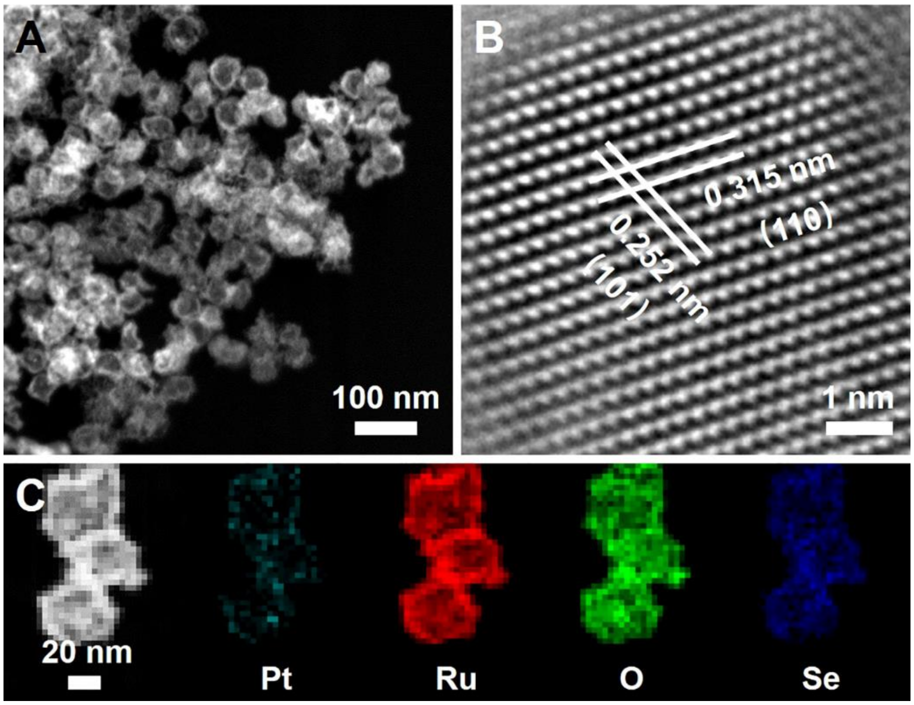

Fig. S13. Morphological and structural analysis. (A) HAADF-STEM image, (B) HRTEM image, and (C) STEM image and STEM-EDS elemental mapping images of 2% Pt-RuO_2 HNSs.

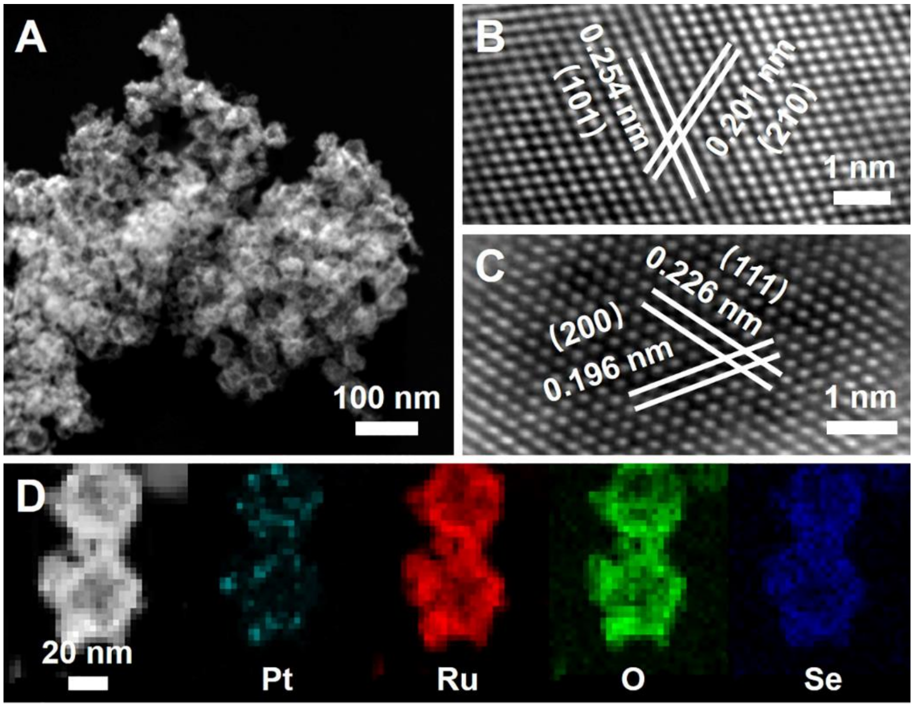

Fig. 14. Morphological and structural analysis. (A) HAADF-STEM image, (B, C) HRTEM images, and (D) STEM image and STEM-EDS elemental mapping images of 10% Pt-RuO_2 HNSs.

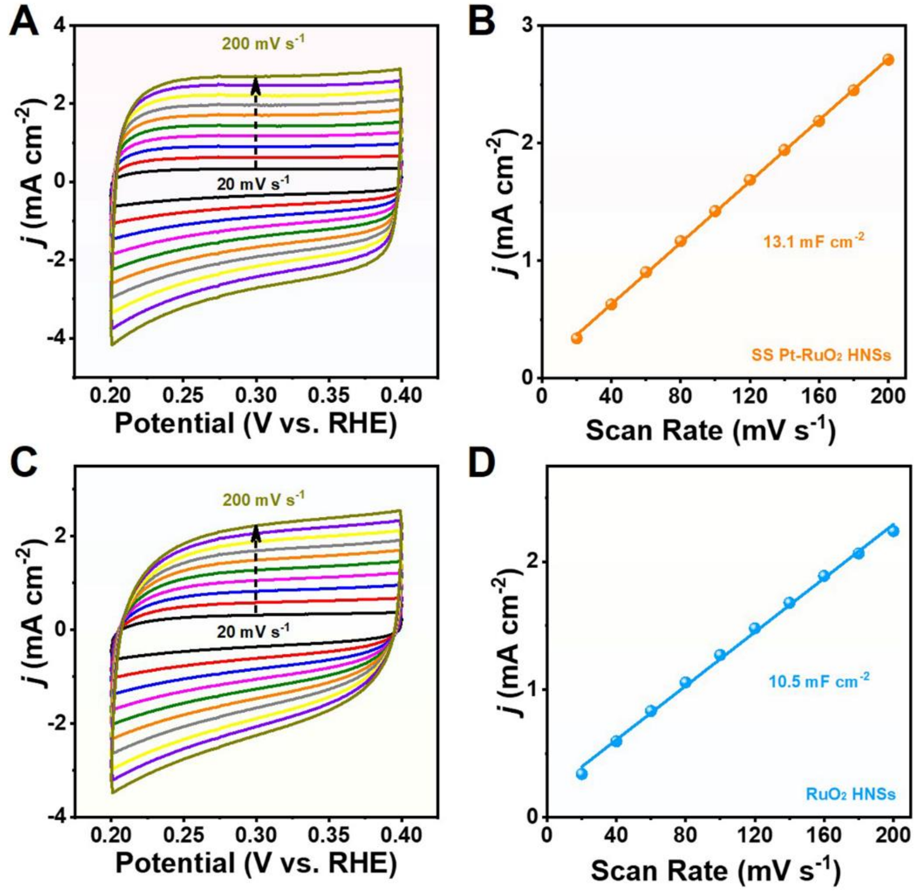

Fig. S15. Catalytic performance over various catalysts. (A, C) Cyclic voltammograms and (B, D) corresponding double layer capacitance (C_{dl}) of (A, B) SS Pt-RuO_2 HNSs and (C, D) RuO_2 HNSs.

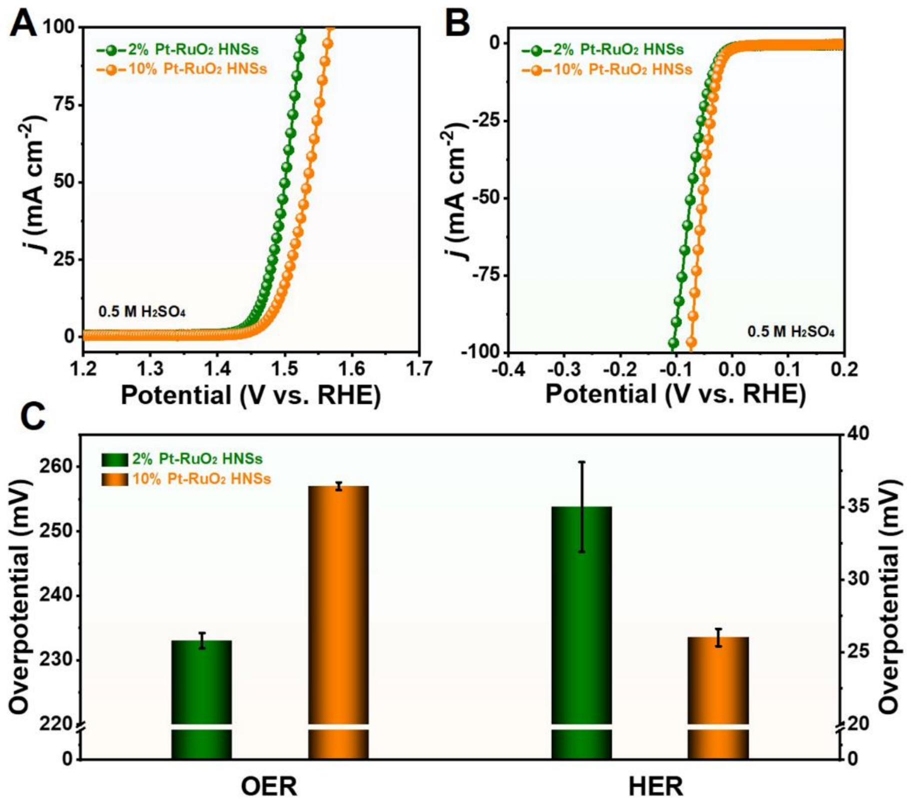

Fig. S16. Catalytic performance over various catalysts. (A) OER polarization curves, (B) HER polarization curves and (C) corresponding histogram of overpotentials at 10 mA cm^{-2} of 2% Pt-RuO_2 HNSs and 10% Pt-RuO_2 HNSs s in 0.5 M H_2SO_4.

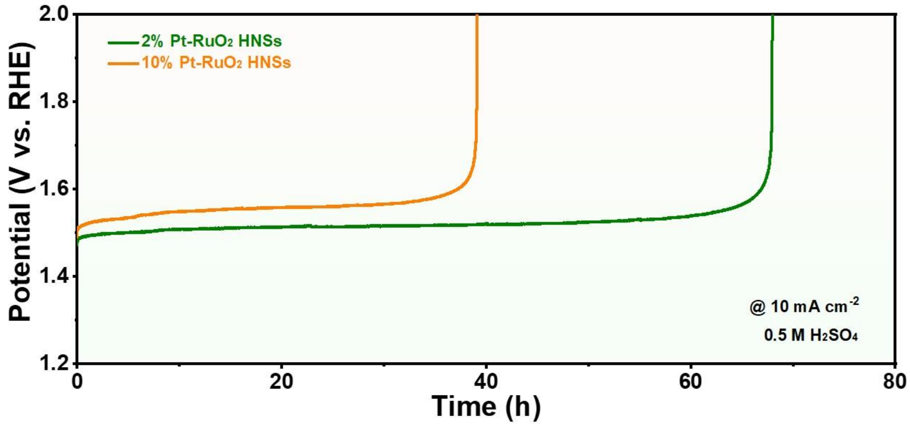

Fig. S17. Stability test for various catalysts. Chronopotentiometry tests of 2% Pt-RuO_2 HNSs and 10% Pt-RuO_2 HNSs in 0.5 M H_2SO_4 at a constant current density of 10 mA cm^{-2}.

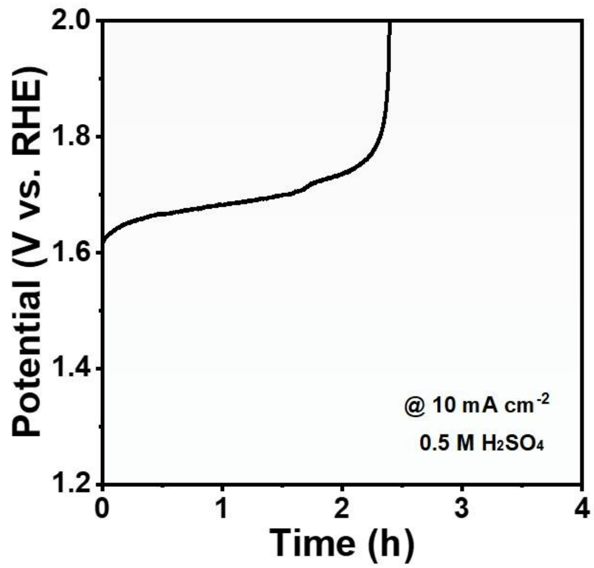

Fig. S18. Stability test of commercial RuO_2 for OER. Chronopotentiometry tests of commercial RuO_2 in 0.5 M H_2SO_4 at a constant current density of 10 mA cm^{-2}.

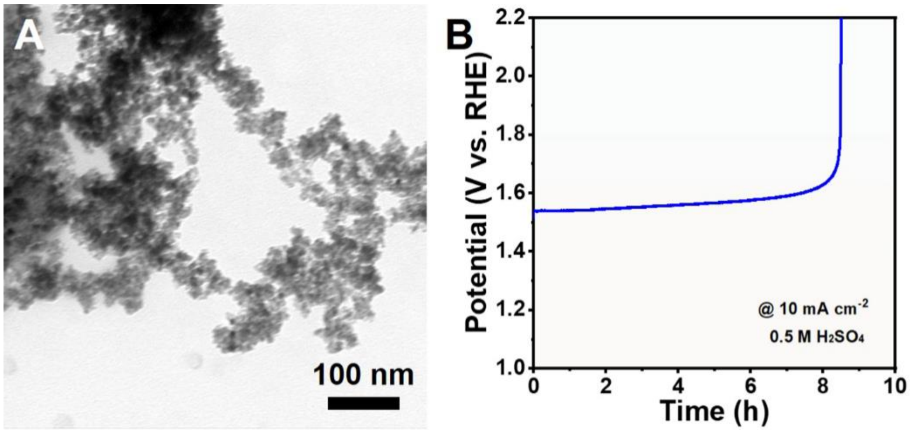

Fig. S19. Stability test of PtRuSe HNSs for OER. (A) TEM image and (B) chronopotentiometry test of PtRuSe HNSs without introducing Vulcan XC-72R C in 0.5 M H_2SO_4 at a constant current density of 10 mA cm^{-2}.

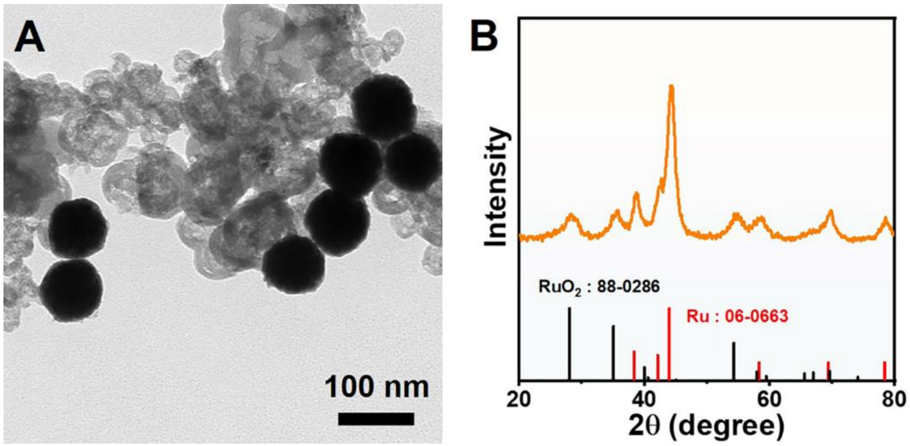

Fig. S20. Morphological and structural analysis. (A) TEM image and (B) XRD pattern of the Pt-Ru solid nanoparticles. Note that H_2SeO_3 was absent during the synthetic process, and the conditions for calcination are same with those of PtRuSe HNSs.

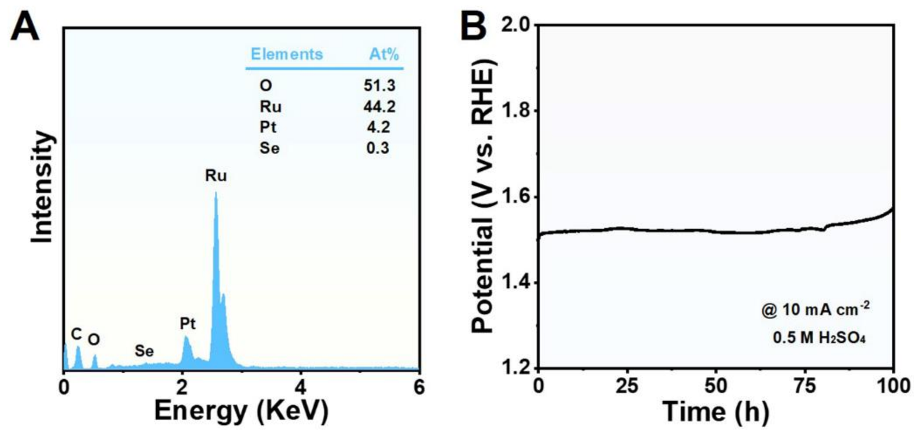

Fig. S21. Effect of residual Se in SS Pt-RuO_2 HNSs for OER. (A) SEM-EDS spectrum and (B) chronopotentiometry test of SS Pt-RuO_2 HNSs (electrochemically leaching of Se) in 0.5 M H_2SO_4 at a constant current density of 10 mA cm^{-2}.

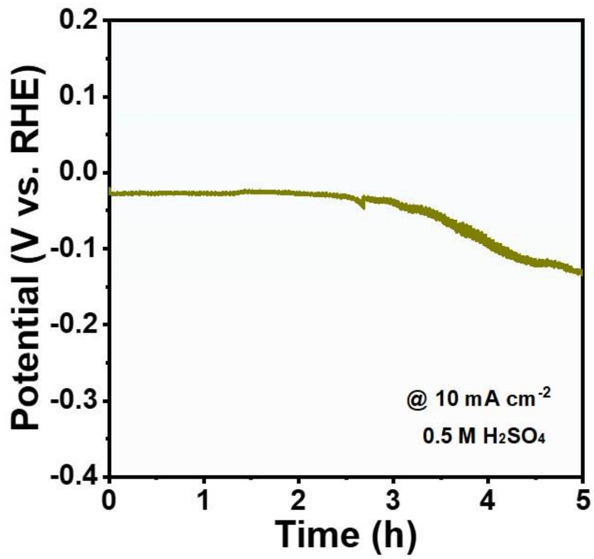

Fig. S22. Stability test of commercial Pt/C for HER. Chronopotentiometry tests of commercial Pt/C in 0.5 M H_2SO_4 at a constant current density of 10 mA cm^{-2}.

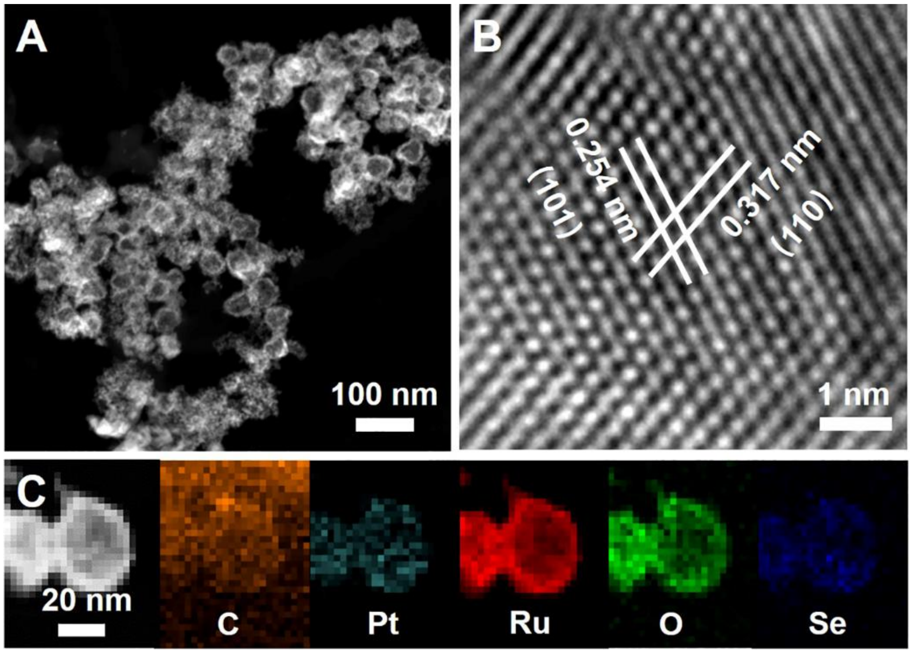

Fig. S23. Morphological and structural analysis of the spent SS Pt-RuO_2 HNSs. (A) HAADF-STEM image, (B) HRTEM image, and (C) STEM image and STEM-EDS elemental mapping images of SS Pt-RuO_2 HNSs after water splitting (cathodic: HER) in 0.5 M H_2SO_4.

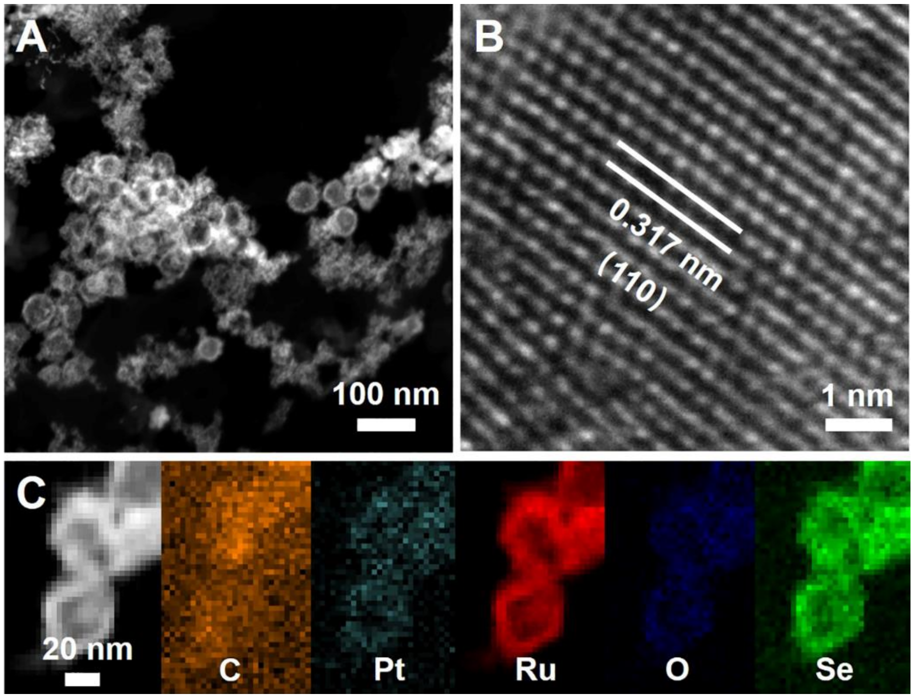

Fig. S24. Morphological and structural analysis of the spent SS Pt-RuO$_2$ HNSs. (A) HAADF-STEM image, (B) HRTEM image, and (C) STEM image and STEM-EDS elemental mapping images of SS Pt-RuO$_2$ HNSs after water splitting (anode: OER) in 0.5 M H_2SO_4.

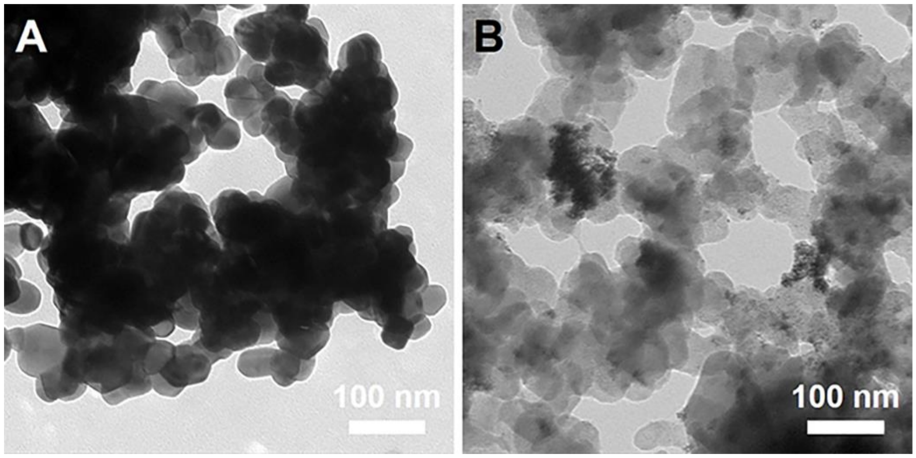

Fig. 25. Morphological analysis of the spent catalysts. TEM images of (A) commercial RuO_2 and (B) commercial Pt/C after water splitting in 0.5 M H_2SO_4.

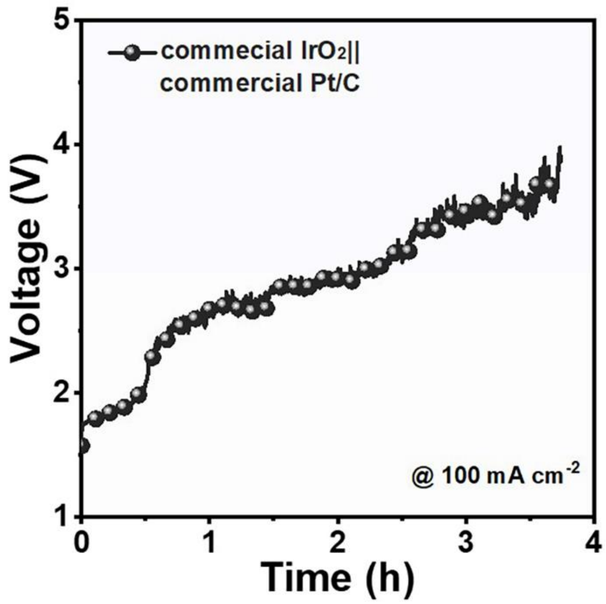

Fig. S26. Stability test of commercial IrO_2 and Pt/C for water splitting. Chronopotentiometry test of commercial IrO_2||commercial Pt/C at a constant current density of 100 mA cm^{-2}.

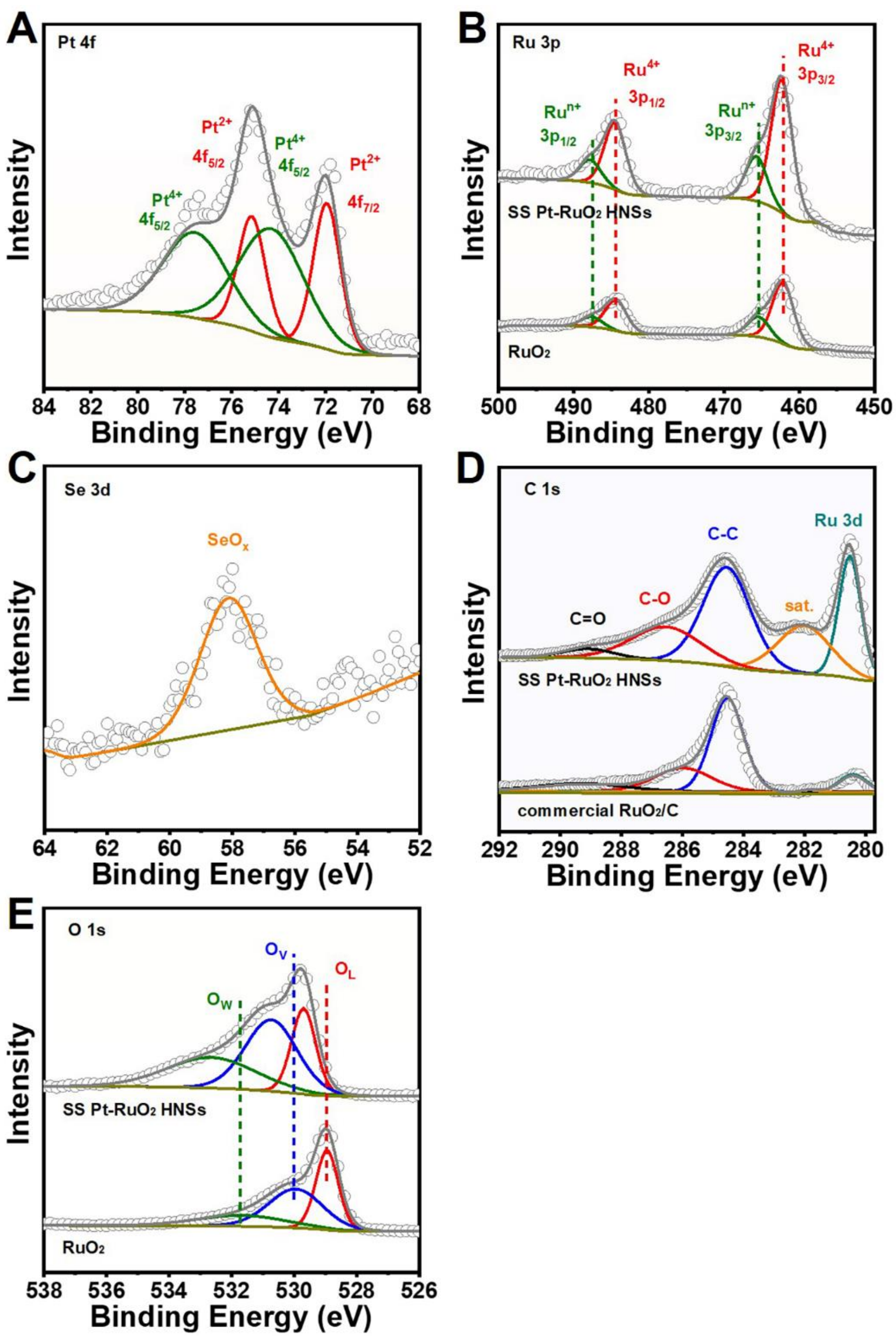

Fig. S27. Structural analysis of SS Pt-RuO_2 HNSs and RuO_2. (A) Pt 4*f* XPS spectrum of SS Pt-RuO_2 HNSs. (B) Ru 3*p* XPS spectra of SS Pt-RuO_2 HNS and RuO_2. (C) Se 3*d* XPS spectrum of SS Pt-RuO_2 HNSs. (D) C 1*s* XPS spectra of SS Pt-RuO_2 HNSs and RuO_2/C (a physical mixture of commercial RuO_2 and VC-X72 C). (E) O 1*s* XPS spectra of SS Pt-RuO_2 HNSs and RuO_2.

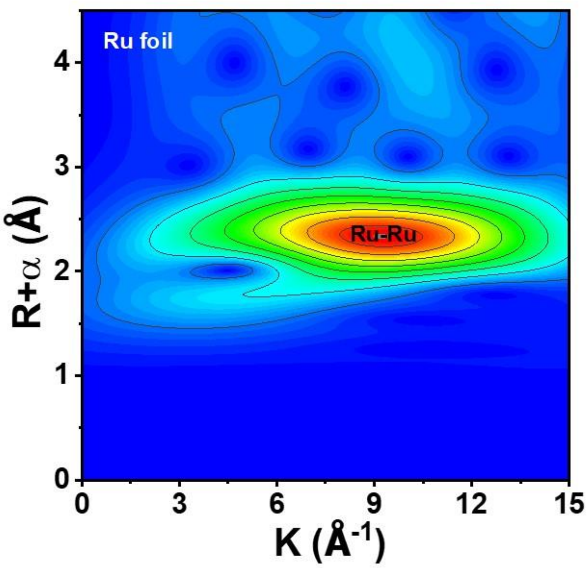

Fig. S28. Structural analysis. Wavelet transform of Ru *K*-edge EXAFS data of Ru foil.

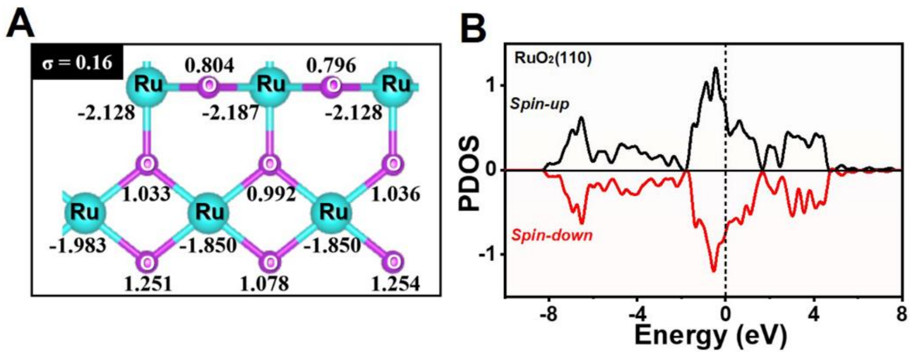

Fig. S29. Theoretical calculations. (**A**) The Bader charge numbers of atoms in RuO_2. Note that the negative value is referred to lose electrons, while the positive value mains to obtain electrons. (**B**) The PDOS of 4*d*-orbitals of surface Ru atoms in RuO_2.

Table S1. Summary of reported OER electrocatalysts in acidic conditions.

Catalyst	Electrolyte	Current density	Overpotential (mV)	Stability (h)	Ref.
SS Pt-RuO_2 HNSs	**0.5 M H_2SO_4**	**10 mA cm^{-2}**	**228**	**100^b**	**This work**
$IrO_x/SrIrO_3$	0.5 M H_2SO_4	10 mA cm^{-2}	~270	30^b	(*51*)
40-IG	0.5 M H_2SO_4	10 mA cm^{-2}	276	4^c	(*52*)
6H-$SrIrO_3$	0.5 M H_2SO_4	10 mA cm^{-2}	248	30^b	(*53*)
P-$IrCu_{1.4}$	0.05 M H_2SO_4	10 mA cm^{-2}	311	10^b	(*54*)
Ru_1-Pt_3Cu	0.1 M $HClO_4$	10 mA cm^{-2}	220	28^b	(*27*)
Ir-STO	0.1 M $HClO_4$	10 mA cm^{-2}	247	20^b	(*55*)
RhCu NTs	0.5 M H_2SO_4	10 mA cm^{-2}	345	12^d	(*56*)
Ir-SA@Fe@NCNT	0.5 M H_2SO_4	10 mA cm^{-2}	250	12^d	(*57*)
a/c-RuO_2	0.1 M $HClO_4$	10 mA cm^{-2}	205	60^b	(*58*)
Ru NWs	0.5 M H_2SO_4	10 mA cm^{-2}	234	20^a	(*59*)
IrRu@Te	0.5 M H_2SO_4	10 mA cm^{-2}	220	20^b	(*60*)
a-PN-IN frame/C	0.1 M $HClO_4$	10 mA cm^{-2}	308	5^a	(*61*)
Li-$IrSe_2$	0.5 M H_2SO_4	10 mA cm^{-2}	220	10^e	(*16*)
Co-RuIr	0.1 M $HClO_4$	10 mA cm^{-2}	235	25^b	(*62*)
RuCu NSs	0.5 M H_2SO_4	10 mA cm^{-2}	236	12^b	(*21*)
Ir-NSG	0.1 M $HClO_4$	10 mA cm^{-2}	265	~1.7^b	(*12*).
$Rh_{22}Ir_{78}$	0.5 M H_2SO_4	10 mA cm^{-2}	292	~8^d	(*63*)
Li-IrO_x	0.5 M H_2SO_4	10 mA cm^{-2}	300	10^b	(*24*)
D-$IrTe_2$ HNSs	0.5 M H_2SO_4	10 mA cm^{-2}	298	~3^b	(*64*)
Ru-N-C	0.5 M H_2SO_4	10 mA cm^{-2}	267	30^d	(*65*)
Ruthenate NSs	0.1 M $HClO_4$	10 mA cm^{-2}	255	~6^b	(*66*)
Amorphous Ir NSs	0.1 M $HClO_4$	10 mA cm^{-2}	255	8^d	(*67*)
$RuNi_2$©G-250	0.5 M H_2SO_4	10 mA cm^{-2}	227	3^b	(*29*)
FeN_x/NF/EG	0.5 M H_2SO_4	10 mA cm^{-2}	294	10^e	(*68*)
$CaCu_3Ru_4O_{12}$	0.5 M H_2SO_4	10 mA cm^{-2}	171	24^b	(*69*)

Note: a, b and c are the chronopotentiometry test at 5, 10 and 20 mA cm^{-2}, respectively. d and e are the chronoamperometry test at 10 and 20 mA cm^{-2}, respectively.

Table S2. Summary of reported HER electrocatalysts in acidic conditions.

Catalyst	Electrolyte	Current density	Overpotential (mV)	Stability (h)	Ref.
SS Pt-RuO$_2$ HNSs	**0.5 M H_2SO_4**	**10 mA cm^{-2}**	**26**	**100^b**	**This work**
Pt$_1$/OLC	0.5 M H_2SO_4	10 mA cm^{-2}	38	100^d	(*70*)
1T$_{0.81}$-MoS$_2$@Ni$_2$P	0.5 M H_2SO_4	10 mA cm^{-2}	38.9	10^d	(*71*)
CoP/NP/TF	0.5 M H_2SO_4	10 mA cm^{-2}	91	10^d	(*72*)
Co-NMGO	0.5 M H_2SO_4	10 mA cm^{-2}	146	24^d	(*73*)
Ce-doped CoP	0.5 M H_2SO_4	10 mA cm^{-2}	54	10^d	(*74*)
IrTiTa	0.5 M H_2SO_4	10 mA cm^{-2}	99	10^b	(*75*)
Ir$_6$Ag$_9$ NTs/C	0.5 M H_2SO_4	10 mA cm^{-2}	20.0	5^a	(*76*)
Ni$_2$P/MoS$_2$/N:RGO	0.5 M H_2SO_4	10 mA cm^{-2}	40	60^e	(*77*)
IrNi NCs	0.1 M $HClO_4$	10 mA cm^{-2}	28	2^a	(*78*)
Co-RuIr	0.1 M $HClO_4$	10 mA cm^{-2}	14	25^b	(*62*)
RhCu NTs	0.5 M H_2SO_4	10 mA cm^{-2}	12	12^d	(*56*)
A-Ni@DG	0.5 M H_2SO_4	10 mA cm^{-2}	70	10^a	(*79*)
RuP$_2$@NPC	0.5 M H_2SO_4	10 mA cm^{-2}	38	11^d	(*80*)
Ir-SA@Fe@NCNT	0.5 M H_2SO_4	10 mA cm^{-2}	26	12^d	(*57*)
W-SAC	0.5 M H_2SO_4	10 mA cm^{-2}	105	~11^d	(*81*)
Mo$_2$C/G-NCS	0.5 M H_2SO_4	10 mA cm^{-2}	~70	20^d	(*82*)
Ni-GF/VC	0.5 M H_2SO_4	10 mA cm^{-2}	111	20^d	(*83*)
Bm-5d-Pt	0.5 M H_2SO_4	10 mA cm^{-2}	30	24^d	(*84*)
RuB$_2$	0.5 M H_2SO_4	10 mA cm^{-2}	52	50^b	(*14*)
Ru@MWCNT	0.5 M H_2SO_4	10 mA cm^{-2}	16	50^e	(*85*)
Pt$_3$Co NPs@NCNT	0.5 M H_2SO_4	10 mA cm^{-2}	42	35^b	(*86*)
Ni@Ni$_2$P-Ru HNRs	0.5 M H_2SO_4	10 mA cm^{-2}	51	~7^b	(*87*)
CBC-Ir-800-1.2	0.5 M H_2SO_4	10 mA cm^{-2}	17	6^b	(*88*)
Ir@N-G-750	0.5 M H_2SO_4	10 mA cm^{-2}	19	20^c	(*89*)
Ru-SA/Ti$_3$C$_2$T$_x$	0.1 M $HClO_4$	10 mA cm^{-2}	70	32^b	(*90*)
Li-PPS NDs	0.5 M H_2SO_4	10 mA cm^{-2}	91	~13^c	(*91*)

Note: a, b and c are the chronopotentiometry test at 5, 10 and 20 mA cm^{-2}, respectively. d and e are the chronoamperometry test at 10 and 20 mA cm^{-2}, respectively.

Table S3. Summary of reported water splitting electrocatalysts in acidic conditions.

Catalyst	Electrolyte	Current density	Voltage (V)	Stability (h)	Ref.
SS Pt-RuO_2 HNSs||SS Pt-RuO_2 HNSs	**0.5 M H_2SO_4**	**10 mA cm^{-2}**	**1.49**	**100^{b}**	**This work**
$RuTe_2$ PNRs||$RuTe_2$ PNRs	0.5 M H_2SO_4	10 mA cm^{-2}	1.52	24^{d}	(*13*)
Ru nanosheets||Ru nanosheets	0.5 M H_2SO_4	10 mA cm^{-2}	1.53	~2^{d}	(*92*)
Mo-Co_9S_8@C	0.5 M H_2SO_4	10 mA cm^{-2}	1.68	24^{d}	(*93*)
Ir-SA@Fe@NCNT||Ir-SA@Fe@NCNT	0.5 M H_2SO_4	10 mA cm^{-2}	1.51	12^{d}	(*57*)
RuB_2||RuB_2	0.5 M H_2SO_4	10 mA cm^{-2}	1.53	~9^{b}	(*14*)
RuCu NSs||RuCu NSs	0.5 M H_2SO_4	10 mA cm^{-2}	1.49	~15^{b}	(*21*)
Ir@N-G-750||Ir@N-G-750	0.5 M H_2SO_4	10 mA cm^{-2}	1.54	40^{c}	(*89*)
RhCu NTs/CP||RhCu NTs/CP	0.5 M H_2SO_4	10 mA cm^{-2}	1.64	30^{d}	(*56*)
Ir_6Ag_9 NTs/C||Ir_6Ag_9 NTs/C	0.5 M H_2SO_4	10 mA cm^{-2}	1.55	~32^{a}	(*76*)
ONPPGC/OCC||ONPPGC/OCC	0.5 M H_2SO_4	5 mA cm^{-2}	1.75	10^{b}	(*94*)
Co-doped RuO_2 NWs||Ni-doped RuO_2 NWs	0.5 M H_2SO_4	10 mA cm^{-2}	1.54	12^{a}	(*22*)
Ir-doped WO_3||Ir-doped WO_3	0.5 M H_2SO_4	10 mA cm^{-2}	1.56	60^{b}	(*95*)
$RuIrO_x$||$RuIrO_x$	0.5 M H_2SO_4	10 mA cm^{-2}	1.45	24^{d}	(*96*)
Li-$IrSe_2$||Li-$IrSe_2$	0.5 M H_2SO_4	10 mA cm^{-2}	1.44	24^{e}	(*16*)
CB[6]-Ir2||CB[6]-Ir2	0.5 M H_2SO_4	10 mA cm^{-2}	1.56	20^{a}	(*97*)
np-IrO_2||*np*-IrAl	0.5 M H_2SO_4	10 mA cm^{-2}	1.52	40^{b}	(*98*)
Co-RuIr||Co-RuIr	0.1 M $HClO_4$	10 mA cm^{-2}	1.52	25^{b}	(*62*)
RuO_2 NWs||Ir NWs	0.5 M H_2SO_4	10 mA cm^{-2}	1.47	10^{a}	(*59*)
$Au_{0.5}Ir_{0.5}$@CNT||$Au_{0.5}Ir_{0.5}$@CNT	0.5 M H_2SO_4	10 mA cm^{-2}	1.51	50^{d}	(*99*)
Ir/GF||Ir/GF	0.5 M H_2SO_4	10 mA cm^{-2}	~1.55	10^{b}	(*100*)
Ru-SA/$Ti_3C_2T_x$||Ru-SA/$Ti_3C_2T_x$	0.1 M $HClO_4$	10 mA cm^{-2}	1.56	32^{b}	(*90*)
$IrNi_{0.57}Fe_{0.82}$||$IrNi_{0.57}Fe_{0.82}$	0.5 M $HClO_4$	10 mA cm^{-2}	1.64	~6^{b}	(*101*)
IrO_x/GDY||IrO_x/GDY	0.5 M H_2SO_4	10 mA cm^{-2}	1.49	30^{d}	(*102*)
Ir-NSG||Ir-NSG	0.1 M $HClO_4$	10 mA cm^{-2}	1.42	24^{b}	(*12*)

Note: a, b and c are the chronopotentiometry test at 5, 10 and 20 mA cm^{-2}, respectively. d and e are the chronoamperometry test at 10 and 20 mA cm^{-2}, respectively.

REFERENCES AND NOTES

1. L. Li, P. Wang, Q. Shao, X. Huang, Metallic nanostructures with low dimensionality for electrochemical water splitting. *Chem. Soc. Rev.* **49**, 3072–3106 (2020).

2. Y. Zhou, S. Sun, C. Wei, Y. Sun, P. Xi, Z. Feng, Z. J. Xu, Significance of engineering the octahedral units to promote the oxygen evolution reaction of spinel oxides. *Adv. Mater.* **31**, 1902509 (2019).

3. C. Wei, S. Sun, D. Mandler, X. Wang, S. Z. Qiao, Z. J. Xu, Approaches for measuring the surface areas of metal oxide electrocatalysts for determining their intrinsic electrocatalytic activity. *Chem. Soc. Rev.* **48**, 2518–2534 (2019).

4. Z. Xiao, Y. C. Huang, C. L. Dong, C. Xie, Z. Liu, S. Du, W. Chen, D. Yan, L. Tao, Z. Shu, G. Zhang, H. Duan, Y. Wang, Y. Zou, R. Chen, S. Wang, Operando identification of the dynamic behavior of oxygen vacancy-rich Co_3O_4 for oxygen evolution reaction. *J. Am. Chem. Soc.* **142**, 12087–12095 (2020).

5. Z. Liu, G. Wang, X. Zhu, Y. Wang, Y. Zou, S. Zang, S. Wang, Optimal geometrical configuration of cobalt cations in spinel oxides to promote oxygen evolution reaction. *Angew. Chem. Int. Ed.* **59**, 4736–4742 (2020).

6. M. Li, K. Duanmu, C. Wan, T. Cheng, L. Zhang, S. Dai, W. Chen, Z. Zhao, P. Li, H. Fei, Y. Zhu, R. Yu, J. Luo, K. Zang, Z. Lin, M. Ding, J. Huang, H. Sun, J. Guo, X. Pan, W. A. Goddard III, P. Sautet, Y. Huang, X. Duan, Single-atom tailoring of platinum nanocatalysts for high-performance multifunctional electrocatalysis. *Nat. Catal.* **2**, 495–503 (2019).

7. L. An, J. Feng, Y. Zhang, R. Wang, H. Liu, G. C. Wang, F. Cheng, P. Xi, Epitaxial heterogeneous interfaces on N-$NiMoO_4$/NiS_2 nanowires/nanosheets to boost hydrogen and oxygen production for overall water splitting. *Adv. Funct. Mater.* **29**, 1805298 (2019).

8. J. X. Feng, H. Xu, S. H. Ye, G. Ouyang, Y. X. Tong, G. R. Li, Silica-polypyrrole hybrids as high-performance metal-free electrocatalysts for the hydrogen evolution reaction in neutral media. *Angew. Chem. Int. Ed.* **56**, 8120–8124 (2017).

9. R. Li, H. Wang, F. Hu, K. C. Chan, X. Liu, Z. Lu, J. Wang, Z. Li, L. Zeng, Y. Li, X. Wu, Y. Xiong, IrW nanochannel support enabling ultrastable electrocatalytic oxygen evolution at 2 A cm^{-2} in acidic media. *Nat. Commun.* **12**, 3540 (2021).

10. A. Ali, P. K. Shen, Recent progress in graphene-based nanostructured electrocatalysts for overall water splitting. *Electrochem. Energy Rev.* **3**, 370–394 (2020).

11. D. Zhao, Z. Zhuang, X. Cao, C. Zhang, Q. Peng, C. Chen, Y. Li, Atomic site electrocatalysts for water splitting, oxygen reduction and selective oxidation. *Chem. Soc. Rev.* **49**, 2215–2264 (2020).

12. Q. Wang, C.-Q. Xu, W. Liu, S.-F. Hung, H. B. Yang, J. Gao, W. Cai, H. M. Chen, J. Li, B. Liu, Coordination engineering of iridium nanocluster bifunctional electrocatalyst for highly efficient and pH-universal overall water splitting. *Nat. Commun.* **11**, 4246 (2020).

13. J. Wang, L. Han, B. Huang, Q. Shao, H. L. Xin, X. Huang, Amorphization activated ruthenium-tellurium nanorods for efficient water splitting. *Nat. Commun.* **10,** 5692 (2019).

14. D. Chen, T. Liu, P. Wang, J. Zhao, C. Zhang, R. Cheng, W. Li, P. Ji, Z. Pu, S. Mu, Ionothermal route to phase-pure RuB_2 catalysts for efficient oxygen evolution and water splitting in acidic media. *ACS Energy Lett.* **5**, 2909–2915 (2020).

15. C. Shang, C. Cao, D. Yu, Y. Yan, Y. Lin, H. Li, T. Zheng, X. Yan, W. Yu, S. Zhou, J. Zeng, Electron correlations engineer catalytic activity of pyrochlore iridates for acidic water oxidation. *Adv. Mater.* **31**, 1805104 (2019).

16. T. Zheng, C. Shang, Z. He, X. Wang, C. Cao, H. Li, R. Si, B. Pan, S. Zhou, J. Zeng, Intercalated iridium diselenide electrocatalysts for efficient pH-universal water splitting. *Angew. Chem. Int. Ed.* **58**, 14764–14769 (2019).

17. J. Li, Y. Wang, T. Zhou, H. Zhang, X. Sun, J. Tang, L. Zhang, A. M. Al-Enizi, Z. Yang, G. Zheng, Nanoparticle superlattices as efficient bifunctional electrocatalysts for water splitting. *J. Am. Chem. Soc.* **137**, 14305–14312 (2015).

18. X. Li, L. Zhao, J. Yu, X. Liu, X. Zhang, H. Liu, W. Zhou, Water splitting: From electrode to green energy system. *Nanomicro Lett.* **12**, 131 (2020).

19. W. Gao, Z. Xia, F. Cao, J. C. Ho, Z. Jiang, Y. Qu, Comprehensive understanding of the spatial configurations of CeO_2 in NiO for the electrocatalytic oxygen evolution reaction: Embedded or surface-loaded. *Adv. Funct. Mater.* **28**, 1706065 (2018).

20. D. Chen, M. Qiao, Y. R. Lu, L. Hao, D. Liu, C. L. Dong, Y. Li, S. Wang, Preferential cation vacancies in perovskite hydroxide for the oxygen evolution reaction. *Angew. Chem. Int. Ed.* **57**, 8691–8696 (2018).

21. Q. Yao, B. Huang, N. Zhang, M. Sun, X. Huang, Channel rich RuCu nanosheets for pH-universal overall water splitting electrocatalysis. *Angew. Chem. Int. Ed.* **58**, 14121–14126 (2019).

22. J. Wang, Y. Ji, R. Yin, Y. Li, Q. Shao, X. Huang, Transition metal-doped ultrathin RuO_2 networked nanowires for efficient overall water splitting across a broad pH range. *J. Mater. Chem. A* **7**, 6411–6416 (2019).

23. G. Meng, W. Sun, A. A. Mon, X. Wu, L. Xia, A. Han, Y. Wang, Z. Zhuang, J. Liu, D. Wang, Y. Li, Strain regulation to optimize the acidic water oxidation performance of atomic-layer IrO_x. *Adv. Mater.* **31**, 1903616 (2019).

24. J. Gao, C. Q. Xu, S. F. Hung, W. Liu, W. Cai, Z. Zeng, C. Jia, H. M. Chen, H. Xiao, J. Li, Y. Huang, B. Liu, Breaking long-range order in iridium oxide by alkali ion for efficient water oxidation. *J. Am. Chem. Soc.* **141**, 3014–3023 (2019).

25. J. Liu, Y. Zheng, Y. Jiao, Z. Wang, Z. Lu, A. Vasileff, S. Z. Qiao, NiO as a bifunctional promoter for RuO_2 toward superior overall water splitting. *Small* **14**, 1704073 (2018).

26. A. Oh, Y. Kim, H. Baik, B. Kim, K. Chaudhari, S. H. Joo, K. Lee, Topotactic transformations in an icosahedral nanocrystal to form efficient water-splitting catalysts. *Adv. Mater.* **31**, 1805546 (2018).

27. Y. Yao, S. Hu, W. Chen, Z. Q. Huang, W. Wei, T. Yao, R. Liu, K. Zang, X. Wang, G. Wu, W. Yuan, T. Yuan, B. Zhu, W. Liu, Z. Li, D. He, Z. Xue, Y. Wang, X. Zheng, J. Dong, C. R. Chang, Y. Chen, X. Hong, J. Luo, S. Wei, W. X. Li, P. Strasser, Y. Wu, Y. Li, Engineering the electronic structure of single atom Ru sites via compressive strain boosts acidic water oxidation electrocatalysis. *Nat. Catal.* **2**, 304–313 (2019).

28. D. Wu, K. Kusada, S. Yoshioka, T. Yamamoto, T. Toriyama, S. Matsumura, Y. Chen, O. Seo, J. Kim, C. Song, S. Hiroi, O. Sakata, T. Ina, S. Kawaguchi, Y. Kubota, H. Kobayashi, H. Kitagawa, Efficient overall water splitting in acid with anisotropic metal nanosheets. *Nat. Commun.* **12**, 1145 (2021).

29. X. Cui, P. Ren, C. Ma, J. Zhao, R. Chen, S. Chen, N. P. Rajan, H. Li, L. Yu, Z. Tian, D. Deng, Robust interface Ru centers for high-performance acidic oxygen evolution. *Adv. Mater.* **32**, 1908126 (2020).

30. J. Sun, R. Ge, K. Jiang, Y. Dong, F. Hao, Z. Tian, G. Chen, L. Chen, Assembling ultrasmall copper-doped ruthenium oxide nanocrystals into hollow porous polyhedra: Highly robust electrocatalysts for oxygen evolution in acidic media. *Adv. Mater.* **30**, 1801351 (2018).

31. J. Shan, C. Guo, Y. Zhu, S. Chen, L. Song, M. Jaroniec, Y. Zheng, S. Z. Qiao, Charge-redistribution-enhanced nanocrystalline Ru@IrO_x electrocatalysts for oxygen evolution in acidic media. *Chem* **5**, 445–459 (2019).

32. Q. Jiang, N. Kurra, M. Alhabeb, Y. Gogotis, H. Alshareef, All pseudocapacitive MXene-RuO_2 asymmetric supercapacitors. *Adv. Energy Mater.* **8**, 1703043 (2018).

33. X. Li, L. Liu, X. Ren, J. Gao, Y. Huang, B. Liu, All microenvironment modulation of single-atom catalysts and their roles in electrochemical energy conversion. *Sci. Adv.* **6**, eabb6833 (2020).

34. N. Cheng, L. Zhang, K. Doyle-Davis, X. Sun, Single-atom catalysts: From design to application. *Electrochem. Energy Rev.* **2**, 539–573 (2019).

35. Y. Zhu, X. Zhu, L. Bu, Q. Shao, Y. Li, Z. Hu, C. T. Chen, C. W. Pao, S. Yang, X. Huang, Single-atom in-doped subnanometer Pt nanowires for simultaneous hydrogen generation and biomass upgrading. *Adv. Funct. Mater.* **30**, 2004310 (2020).

36. Y. Lin, Z. Tian, L. Zhang, J. Ma, Z. Jiang, B. Deibert, R. Ge, L. Chen, Chromium-ruthenium oxide solid solution electrocatalyst for highly efficient oxygen evolution reaction in acidic media. *Nat. Commun.* **10**, 162 (2019).

37. X. Wang, L. Zhuang, Y. Jia, H. Liu, X. Yan, L. Zhang, D. Yang, Z. Zhu, X. Yao, Plasma-triggered synergy of exfoliation, phase transformation, and surface engineering in cobalt diselenide for enhanced water oxidation. *Angew. Chem. Int. Ed.* **57**, 16421–16425 (2018).

38. Z. Wu, Y. Zhao, W. Jin, B. Jia, J. Wang, T. Ma, Recent progress of vacancy engineering for electrochemical energy conversion related applications. *Adv. Funct. Mater.* **31**, 2009070 (2021).

39. X. Yan, Y. Jia, X. Yao, Defective structures in metal compounds for energy-related electrocatalysis. *Small Struct.* **2**, 2000067 (2021).

40. Z. Hu, H. Von Lips, M. S. Golden, J. Fink, G. Kaindl, F. M. F. de Groot, S. Ebbinghaus, A. Reller, Multiplet effects in the Ru $L_{2,3}$ x-ray-absorption spectra of Ru(IV) and Ru(V) compounds. *Phys. Rev. B* **61**, 5262–5266 (2000).

41. J. Zhou, J. Wang, H. Fang, C. Wu, J. N. Cutler, T. K. Sham, Nanoscale chemical imaging and spectroscopy of individual RuO_2 coated carbon nanotubes. *Chem. Commun.* **46**, 2778–2780 (2010).

42. H. Sun, Z. Yan, F. Liu, W. Xu, F. Cheng, J. Chen, Self-supported transition-metal-based electrocatalysts for hydrogen and oxygen evolution. *Adv. Mater.* **32**, 1806326 (2019).

43. S. Hao, M. Liu, J. Pan, X. Liu, X. Tan, N. Xu, Y. He, L. Lei, X. Zhang, Dopants fixation of ruthenium for boosting acidic oxygen evolution stability and activity. *Nat. Commun.* **11**, 5368 (2020).

44. V. Viswanathan, H. A. Hansen, J. Rossmeisl, J. K. Nørskov, Unifying the $2e^{-}$ and $4e^{-}$ reduction of oxygen on metal surfaces. *J. Phys. Chem. Lett.* **3**, 2948–2951 (2012).

45. G. Kresse, J. Furthmüller, Efficient iterative schemes for ab initio total-energy calculations using a plane-wave basis set. *Phys. Rev. B* **54**, 11169–11186 (1996).

46. J. P. Perdew, J. A. Chevary, S. H. Vosko, K. A. Jackson, M. R. Pederson, D. J. Singh, C. Fiolhais, Atoms, molecules, solids, and surfaces: Applications of the generalized gradient approximation for exchange and correlation. *Phys. Rev. B Condens. Matter* **46**, 6671–6687 (1992).

47. J. P. Perdew, J. A. Chevary, S. H. Vosko, K. A. Jackson, M. R. Pederson, D. J. Singh, C. Fiolhais, Erratum: Atoms, molecules, solids, and surfaces: Applications of the generalized gradient approximation for exchange and correlation. *Phys. Rev. B Condens. Matter* **48**, 4978 (1993).

48. S. Wang, E. Zhu, Y. Huang, H. Heinz, Direct correlation of oxygen adsorption on platinum-electrolyte interfaces with the activity in the oxygen reduction reaction. *Sci. Adv.* **7**, eabb1435 (2021).

49. S. Grimme, S. Ehrlich, L. Goerigk, Effect of the damping function in dispersion corrected density functional theory. *J. Comput. Chem.* **32**, 1456–1465 (2011).

50. W. Malcolm, J. R. Chase, *NIST-JANAF Thermochemical Tables* (American Institute of Physics, 1998).

51. L. C. Seitz, C. F. Dickens, K. Nishio, Y. Hikita, J. Montoya, A. Doyle, C. Kirk, A. Vojvodic, H. Y. Hwang, J. K. Norskov, T. F. Jaramillo, A highly active and stable $IrO_x/SrIrO_3$ catalyst for the oxygen evolution reaction. *Science* **353**, 1011–1014 (2016).

52. J. Chen, P. Cui, G. Zhao, K. Rui, M. Lao, Y. Chen, X. Zheng, Y. Jiang, H. Pan, S. X. Dou, W. Sun, Low-coordinate iridium oxide confined on graphitic carbon nitride for highly efficient oxygen evolution. *Angew. Chem. Int. Ed.* **58**, 12540–12544 (2019).

53. L. Yang, G. Yu, X. Ai, W. Yan, H. Duan, W. Chen, H. Duan, X. Li, T. Wang, C. Zhang, X. Huang, J. S. Chen, X. Zou, Efficient oxygen evolution electrocatalysis in acid by a perovskite with face-sharing IrO_6 octahedral dimers. *Nat. Commun.* **9**, 5236 (2018).

54. Y. Pi, J. Guo, Q. Shao, X. Huang, Highly efficient acidic oxygen evolution electrocatalysis enabled by porous Ir-Cu nanocrystals with three-dimensional electrocatalytic surfaces. *Chem. Mater.* **30**, 8571–8578 (2018).

55. X. Liang, L. Shi, Y. Liu, H. Chen, R. Si, W. Yan, Q. Zhang, G. D. Li, L. Yang, X. Zou, Activating inert, nonprecious perovskites with iridium dopants for efficient oxygen evolution reaction under acidic conditions. *Angew. Chem. Int. Ed.* **131**, 7713–7717 (2019).

56. D. Cao, H. Xu, D. Cheng, Construction of defect-Rich RhCu nanotubes with highly active Rh_3Cu_1 alloy phase for overall water splitting in all pH values. *Adv. Energy Mater.* **10**, 1903038 (2020).

57. F. Luo, H. Hu, X. Zhao, Z. Yang, Q. Zhang, J. Xu, T. Kaneko, Y. Yoshida, C. Zhu, W. Cai, Robust and stable acidic overall water splitting on Ir single atoms. *Nano Lett.* **20**, 2120–2128 (2020).

58. L. Zhang, H. Jang, H. Liu, M. G. Kim, D. Yang, S. Liu, X. Liu, J. Cho, Sodium-decorated amorphous/crystalline RuO_2 with rich oxygen vacancies: A robust pH-universal oxygen evolution electrocatalyst. *Angew. Chem. Int. Ed.* **60**, 18821–18829 (2021).

59. J. Yang, Y. Ji, Q. Shao, N. Zhang, Y. Li, X. Huang, A universal strategy to metal wavy nanowires for efficient electrochemical water splitting at pH-universal conditions. *Adv. Funct. Mater.* **28**, 1803722 (2018).

60. J. Xu, Z. Lian, B. Wei, Y. Li, O. Bondarchuk, N. Zhang, Z. Yu, A. Araujo, I. Amorim, Z. Wang, B. Li, L. Liu, Strong electronic coupling between ultrafine iridium−ruthenium nanoclusters and conductive, acid-stable tellurium nanoparticle support for efficient and durable oxygen evolution in acidic and neutral media. *ACS Catal.* **10**, 3571–3579 (2020).

61. S. Choi, J. Park, M. K. Kabiraz, Y. Hong, T. Kwon, T. Kim, A. Oh, H. Baik, M. Lee, S.-M. Peak, S.-I. Choi, K. Lee, Pt dopant: Controlling the Ir oxidation states toward efficient and durable oxygen evolution reaction in acidic media. *Adv. Funct. Mater.* **30**, 2003935 (2020).

62. J. Shan, T. Ling, K. Davey, Y. Zheng, S. Z. Qiao, Transition-metal-doped RuIr bifunctional nanocrystals for overall water splitting in acidic environments. *Adv. Mater.* **31**, 1900510 (2019).

63. H. Guo, Z. Fang, H. Li, D. Fernandez, G. Henkelman, S. M. Humphrey, G. Yu. Rational design of rhodium−iridium alloy nanoparticles as highly active catalysts for acidic oxygen evolution. *ACS Nano* **13**, 13225–13234 (2019).

64. Y. Pi, Y. Xu, L. Li, T. Sun, B. Huang, L. Bu, Y. Ma, Z. Hu, C. W. Pao, X. Huang, Selective surface reconstruction of a defective iridium-based catalyst for high-efficiency water splitting. *Adv. Funct. Mater.* **30**, 2004375 (2020).

65. L. Cao, Q. Luo, J. Chen, L. Wang, Y. Lin, H. Wang, X. Liu, X. Shen, W. Zhang, W. Liu, Z. Qi, Z. Jiang, J. Yang, T. Yao, Dynamic oxygen adsorption on single-atomic ruthenium catalyst with high performance for acidic oxygen evolution reaction. *Nat. Commun.* **10**, 4849 (2019).

66. S. Laha, Y. Lee, F. Podjaski, D. Weber, V. Duppel, L. M. Schoop, F. Pielhofer, C. Scheurer, K. Müller, U. Starke, K. Reuter, B. V. Lotsch, Ruthenium oxide nanosheets for enhanced oxygen evolution catalysis in acidic medium. *Adv. Energy Mater.* **9**, 1803795 (2019).

67. G. Wu, X. Zheng, P. Cui, H. Jiang, X. Wang, Y. Qu, W. Chen, Y. Lin, H. Li, X. Han, Y. Hu, P. Liu, Q. Zhang, J. Ge, Y. Yao, R. Sun, Y. Wu, L. Gu, X. Hong, Y. Li, A general synthesis approach for amorphous noble metal nanosheets. *Nat. Commun.* **10**, 4855 (2019).

68. C. Lei, H. Chen, J. Cao, J. Yang, M. Qiu, Y. Xia, C. Yuan, B. Yang, Z. Li, X. Zhang, L. Lei, J. Abbott, Y. Zhong, X. Xia, G. Wu, Q. He, Y. Hou, FeN_4 sites embedded into carbon nanofiber integrated with electrochemically exfoliated graphene for oxygen evolution in acidic medium. *Adv. Energy Mater.* **8**, 1801912 (2018).

69. X. Miao, L. Zhang, L. Wu, Z. Hu, L. Shi, S. Zhou, Quadruple perovskite ruthenate as a highly efficient catalyst for acidic water oxidation. *Nat. Commun.* **10**, 3809 (2019).

70. D. Liu, X. Li, S. Chen, H. Yan, C. Wang, C. Wu, Y. A. Haleem, S. Duan, J. Lu, B. Ge, P. M. Ajayan, Y. Luo, J. Jiang, L. Song, Atomically dispersed platinum supported on curved carbon supports for efficient electrocatalytic hydrogen evolution. *Nat. Energy* **4**, 512–518 (2019).

71. M. Liu, J. A. Wang, W. Klysubun, G. G. Wang, S. Sattayaporn, F. Li, Y. W. Cai, F. Zhang, J. Yu, Y. Yang, Interfacial electronic structure engineering on molybdenum sulfide for robust dual-pH hydrogen evolution. *Nat. Commun.* **12**, 5260 (2021).

72. X. Huang, X. Xu, C. Li, D. Wu, D. Cheng, D. Cao, Vertical CoP nanoarray wrapped by N, P-doped carbon for hydrogen evolution reaction in both acidic and alkaline conditions. *Adv. Energy Mater.* **9**, 1803970 (2019).

73. K. Khan, T. Liu, M. Arif, X. Yan, M. D. Hossain, F. Rehman, S. Zhou, J. Yang, C. Sun, S. H. Bae, J. Kim, K. Amine, X. Pan, Z. Luo, Laser-irradiated holey graphene-supported single-atom catalyst towards hydrogen evolution and oxygen reduction. *Adv. Energy Mater.* **11**, 21001619 (2021).

74. W. Gao, M. Yan, H. Y. Cheung, Z. Xia, X. Zhou, Y. Qin, C. Y. Wong, J. C. Ho, C. R. Chang, Y. Qu, Modulating electronic structure of CoP electrocatalysts towards enhanced hydrogen evolution by Ce chemical doping in both acidic and basic media. *Nano Energy* **38**, 290–296 (2017).

75. Z. J. Wang, M. X. Li, J. H. Yu, X. B. Ge, Y. H. Liu, W. H. Wang, Low-iridium-content IrNiTa metallic glass films as intrinsically active catalysts for hydrogen evolution reaction. *Adv. Mater.* **32**, 1906384 (2020).

76. M. Zhu, Q. Shao, Y. Qian, X. Huang, Superior overall water splitting electrocatalysis in acidic conditions enabled by bimetallic Ir-Ag nanotubes. *Nano Energy* **56**, 330–337 (2019).

77. M. Kim, M. A. R. Anjum, M. Lee, B. J. Lee, J. S. Lee, Activating MoS_2 basal plane with Ni_2P nanoparticles for Pt-like hydrogen evolution reaction in acidic media. *Adv. Funct. Mater.* **29**, 1809151 (2019).

78. Y. Pi, Q. Shao, P. Wang, J. Guo, X. Huang, General formation of monodisperse IrM (M = Ni, Co, Fe) bimetallic nanoclusters as bifunctional electrocatalysts for acidic overall water splitting. *Adv. Funct. Mater.* **27**, 1700886 (2017).

79. L. Zhang, Y. Jia, G. Gao, X. Yan, N. Chen, J. Chen, M. T. Soo, B. Wood, D. Yang, A. Du, X. Yao, Graphene defects trap atomic Ni species for hydrogen and oxygen evolution reactions. *Chem* **4**, 285–297 (2018).

80. Z. Pu, I. S. Amiinu, Z. Kou, W. Li, S. Mu, RuP_2-based catalysts with platinum-like activity and higher durability for the hydrogen evolution reaction at all pH values. *Angew. Chem. Int. Ed.* **56**, 11559–11564 (2017).

81. W. Chen, J. Pei, C.-T. He, J. Wan, H. Ren, Y. Wang, J. Dong, K. Wu, W.-C. Cheong, J. Mao, X. Zheng, W. Yan, Z. Zhuang, C. Chen, Q. Peng, D. Wang, Y. Li, Single tungsten atoms supported on MOF-derived N-doped carbon for robust electrochemical hydrogen evolution. *Adv. Mater.* **30**, 1800396 (2018).

82. H. Wei, Q. Xi, X. Chen, D. Guo, F. Ding, Z. Yang, S. Wang, J. Li, S. Huang, Molybdenum carbide nanoparticles coated into the graphene wrapping N-doped porous carbon microspheres for highly efficient electrocatalytic hydrogen evolution both in acidic and alkaline media. *Adv. Sci.* **5**, 1700733 (2018).

83. C. Yang, R. Zhao, H. Xiang, J. Wu, W. Zhong, W. Li, Q. Zhang, N. Yang, X. Li, Ni-activated transition metal carbides for efficient hydrogen evolution in acidic and alkaline solutions. *Adv. Energy Mater.* **10**, 2002260 (2020).

84. C. Zhang, Y. Cui, Y. Yang, L. Lu, S. Yu, Z. Meng, Y. Wu, Y. Li, Y. Wang, H. Tian, W. Zheng, Highly conductive amorphous pentlandite anchored with ultrafine platinum

nanoparticles for efficient pH-universal hydrogen evolution reaction. *Adv. Funct. Mater.* **27**, 2105372 (2021).

85. D. H. Kweon, M. S. Okyay, S.-J. Kim, J.-P. Jeon, H.-J. Noh, N. Park, J. Mahmood, J.-B. Baek, Ruthenium anchored on carbon nanotube electrocatalyst for hydrogen production with enhanced Faradaic efficiency. *Nat. Commun.* **11**, 1278 (2021).

86. S. L. Zhang, X. F. Lu, Z.-P. Wu, D. Luan, X. W. Lou, Engineering platinum–cobalt nano-alloys in porous nitrogen-doped carbon nanotubes for highly efficient electrocatalytic hydrogen evolution. *Angew. Chem. Int. Ed.* **60**, 19068–19073 (2021).

87. Y. Liu, S. Liu, Y. Wang, Q. Zhang, L. Gu, S. Zhao, D. Xu, Y. Li, J. Bao, Z. Dai, Ru modulation effects in the synthesis of unique rod-like Ni@Ni_2P–Ru heterostructures and their remarkable electrocatalytic hydrogen evolution performance. *J. Am. Chem. Soc.* **140**, 2731–2734 (2018).

88. X. Xiao, H. Zhang, Y. Xiong, F. Liang, Y. W. Yang, Iridium-doped N-rich mesoporous carbon electrocatalyst with synthetic macrocycles as carbon source for hydrogen evolution reaction. *Adv. Funct. Mater.* **31**, 2105562 (2021).

89. X. Wu, B. Feng, W. Li, Y. Niu, Y. Yu, S. Lu, C. Zhong, P. Liu, Z. Tian, L. Chen, W. Hu, C. M. Li, Metal-support interaction boosted electrocatalysis of ultrasmall iridium nanoparticles supported on nitrogen doped graphene for highly efficient water electrolysis in acidic and alkaline media. *Nano Energy* **62**, 117–126 (2019).

90. X. Peng, S. Zhao, Y. Mi, L. Han, X. Liu, D. Qi, J. Sun, Y. Liu, H. Bao, L. Zhuo, H. L. Xin, J. Luo, X. Sun, Trifunctional single-atomic Ru sites enable efficient overall water splitting and oxygen reduction in acidic media. *Small* **16**, 2002888 (2020).

91. X. Zhang, Z. Luo, P. Yu, Y. Cai, Y. Du, D. Wu, S. Gao, C. Tan, Z. Li, M. Ren, T. Osipowicz, S. Chen, Z. Jiang, J. Li, Y. Huang, J. Yang, Y. Chen, C. Y. Ang, Y. Zhao, P. Wang, L. Song, X. Wu, Z. Liu, A. Borgna, H. Zhang, Lithiation-induced amorphization of $Pd_3P_2S_8$ for highly efficient hydrogen evolution. *Nat. Catal.* **1**, 460–468 (2018).

92. X. Kong, K. Xu, C. Zhang, J. Dai, S. Norooz Oliaee, L. Li, X. Zeng, C. Wu, Z. Peng, Free-standing two-dimensional Ru nanosheets with high activity toward water splitting. *ACS Catal.* **6**, 1487–1492 (2016).

93. L. Wang, X. Duan, X. Liu, L. Gu, R. Si, Y. Qiu, Y. Qiu, D. Shi, F. Chen, X. Sun, J. Lin, J. Sun, Atomically dispersed Mo supported on metallic Co_9S_8 nanoflakes as an advanced noble-metal-free bifunctional water splitting catalyst working in universal pH conditions. *Adv. Energy Mater.* **10**, 1903137 (2020).

94. J. Lai, S. Li, F. Wu, M. Saqib, R. Luque, G. Xu, Unprecedented metal-free 3D porous carbonaceous electrodes for full water splitting. *Energ. Environ. Sci.* **9**, 1210–1214 (2016).

95. P. Li, X. Duan, Y. Kuang, X. Sun, Iridium in tungsten trioxide matrix as an efficient bi-functional electrocatalyst for overall water splitting in acidic media. *Small* **17**, 2102078 (2021).

96. Z. Zhuang, Y. Wang, C. Q. Xu, S. Liu, C. Chen, Q. Peng, Z. Zhuang, H. Xiao, Y. Pan, S. Lu, R. Yu, W. C. Cheong, X. Cao, K. Wu, K. Sun, Y. Wang, D. Wang, J. Li, Y. Li, Three-dimensional open nano-netcage electrocatalysts for efficient pH-universal overall water splitting. *Nat. Commun.* **10**, 4875 (2019).

97. H. You, D. Wu, Z. Chen, F. Sun, H. Zhang, Z. Chen, M. Cao, W. Zhuang, R. Cao, Highly active and stable water splitting in acidic media using a bifunctional iridium/cucurbit[6]uril catalyst. *ACS Energy Lett.* **4**, 1301–1307 (2019).

98. Q. Li, J. Li, J. Xu, N. Zhang, Y. Li, L. Liu, D. Pan, Z. Wang, F. L. Deepak, Ultrafine-grained porous Ir-based catalysts for high-performance overall water splitting in acidic media. *ACS Appl. Energy Mater.* **3**, 3736–3744 (2020).

99. H. Hu, F. M. D. Kazim, Z. Ye, Y. Xie, Q. Zhang, K. Qu, J. Xu, W. Cai, S. Xiao, Z. Yang, Electronically delocalized Ir enables efficient and stable acidic water splitting. *J. Mater. Chem. A* **8**, 20168–20174 (2020).

100. J. Zhang, G. Wang, Z. Liao, P. Zhang, F. Wang, X. Zhuang, E. Zschech, X. Feng, Iridium nanoparticles anchored on 3D graphite foam as a bifunctional electrocatalyst for excellent overall water splitting in acidic solution. *Nano Energy* **40**, 27–33 (2017).

101. L. Fu, G. Cheng, W. Luo, Colloidal synthesis of monodisperse trimetallic IrNiFe nanoparticles as highly active bifunctional electrocatalysts for acidic overall water splitting. *J. Mater. Chem. A* **5**, 24836–24841 (2017).

102. Z. Wang, Z. Zheng, Y. Xue, F. He, Y. Li, Acidic water oxidation on quantum dots of IrO_x/graphdiyne. *Adv. Energy Mater.* **11**, 2101138 (2017).